




Zinc(II) complexes derived from imidazo[1,2-a]pyridin-2-ylacetic acid (HIP-2-ac): [Zn(IP-2-ac)₂(H₂O)] and unexpectedly, [Zn₃(IP-2-ac)₆(H₂O)]·11H₂O

Agnieszka Dylong, Michał Sowa, Waldemar Goldeman, Katarzyna Ślepokura, Piotr Drożdżewski, Bogumiła Szponar & Ewa Matczak-Jon


To cite this article: Agnieszka Dylong, Michał Sowa, Waldemar Goldeman, Katarzyna Ślepokura, Piotr Drożdżewski, Bogumiła Szponar & Ewa Matczak-Jon (2015) Zinc(II) complexes derived from imidazo[1,2-a]pyridin-2-ylacetic acid (HIP-2-ac): [Zn(IP-2-ac)₂(H₂O)] and unexpectedly, [Zn₃(IP-2-ac)₆(H₂O)]·11H₂O, Journal of Coordination Chemistry, 68:13, 2208-2224, DOI: [10.1080/00958972.2015.1048241](https://doi.org/10.1080/00958972.2015.1048241)

To link to this article: <http://dx.doi.org/10.1080/00958972.2015.1048241>

 View supplementary material 

 Accepted author version posted online: 06 May 2015.
Published online: 08 Jun 2015.

 Submit your article to this journal 

 Article views: 101

 View related articles 

 View Crossmark data 

Zinc(II) complexes derived from imidazo[1,2-a]pyridin-2-ylacetic acid (*HIP-2-ac*): $[\text{Zn}(\text{IP-2-ac})_2(\text{H}_2\text{O})]$ and unexpectedly, $[\text{Zn}_3(\text{IP-2-ac})_6(\text{H}_2\text{O})] \cdot 11\text{H}_2\text{O}$

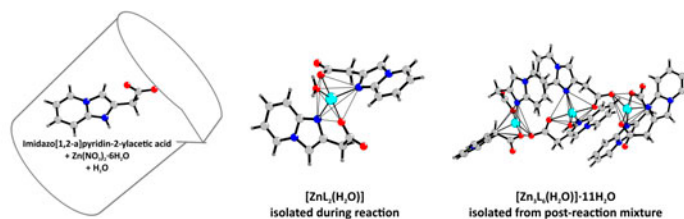
AGNIESZKA DYLONG[†], MICHAŁ SOWA[†], WALDEMAR GOLDEMAN[†],
KATARZYNA ŚLEPOKURA[‡], PIOTR DROŹDŹEWSKI[†], BOGUMIŁA SZPONAR[§] and
EWA MATCZAK-JON^{*†}

[†]Department of Chemistry, Wrocław University of Technology, Wrocław, Poland

[‡]Faculty of Chemistry, University of Wrocław, Wrocław, Poland

[§]Ludwik Hirszfeld Institute of Immunology and Experimental Therapy, Polish Academy of Sciences, Wrocław, Poland

(Received 30 January 2015; accepted 13 April 2015)



Two zinc(II) complexes based on imidazo[1,2-a]pyridin-2-ylacetate (*IP-2-ac*), $[\text{Zn}(\text{IP-2-ac})_2(\text{H}_2\text{O})]$ (**1**) and $[\text{Zn}_3(\text{IP-2-ac})_6(\text{H}_2\text{O})] \cdot 11\text{H}_2\text{O}$ (**2**), were synthesized and characterized by single-crystal X-ray diffraction. In both **1** and **2**, zinc(II) ions are five-coordinate with N_2O_3 donor set, best described as a distorted trigonal-bipyramidal geometry. In **1**, two *IP-2-ac* ligands chelate zinc(II) through a *N,O* donor set, whereas in **2**, both bidentate and μ -bridging binding modes of *IP-2-ac* are observed. The crystal of **1** comprises discrete $\text{Zn}(\text{IP-2-ac})_2(\text{H}_2\text{O})$ coordination entities combined into layers by hydrogen bonds. Inter-layer stabilization of the 3-D crystal lattice is provided by weak $\text{C-H}\cdots\text{O}$ contacts and $\pi\cdots\pi$ interactions. The structure of **2** consists of discrete trinuclear $\text{Zn}_3(\text{IP-2-ac})_6(\text{H}_2\text{O})$ coordination entities joined into crystal lattice by multiple water molecules.

Compound **1** was characterized by FTIR and FT-Raman spectroscopy, and in terms of thermal stability. Furthermore, its antibacterial activity was tested against selected gram-positive, gram-negative bacteria, and *Candida albicans* yeast and compared with activity of previously reported $[\text{M}(\text{IP-2-ac})_2(\text{H}_2\text{O})_2] \cdot 2\text{H}_2\text{O}$ ($\text{M} = \text{Co}, \text{Ni}, \text{Mn}, \text{Cd}$) complexes.

Keywords: Imidazo[1,2-a]pyridine; Zinc(II) complexes; X-ray structures; Vibrational spectra; Thermal stability; Antibacterial activity

*Corresponding author. Email: ewa.maczak-jon@pwr.edu.pl

1. Introduction

Fused nitrogen-containing heterocyclic systems are ubiquitous in nature and play a significant role in pharmaceutical industry and materials science [1–4]. A class of compounds that proved their pharmaceutical importance are imidazo[1,2-a]pyridine (IP) derivatives [2], a number of which, including zolpidem (a sedative) [5], alpidem (an anxiolytic) [6], olprinone (a cardiotonic agent) [7], and minodronic acid (antiresorptive agent) [8], are already available in the market as commercial drugs. Furthermore, many compounds incorporating the IP scaffold have revealed their potential as antimicrobial agents [9].

Surprisingly, the coordination chemistry of IP derivatives has received little attention. Reports are mostly devoted to stable anion radicals such as (bipo)^{•-} and (obip)^{•-}, which have been used for the preparation of coordination polymers with interesting luminescence and magnetic properties [3, 4]. Furthermore, organotin(IV) complexes of IP, and rhodium and iridium complexes of *N*-heterocyclic carbenes containing IP ring have been reported [10].

Recently, using imidazo[1,2-a]pyridin-2-ylacetic acid (*HIP-2-ac*), we have synthesized a series of discrete isostructural [M(*IP-2-ac*)₂(H₂O)₂] \cdot 2H₂O (M = Co, Ni, Mn, Cd) coordination compounds, in which M(II) ions are six-coordinate by two *trans*-oriented bidentate *IP-2-ac* anions and two water molecules [11]. Thermal analysis revealed that the studied compounds release crystallization and coordinated water in different manners, resulting in the lowest thermal stability of [Co(*IP-2-ac*)₂(H₂O)₂] \cdot 2H₂O and the highest thermal stability of [Cd(*IP-2-ac*)₂(H₂O)₂] \cdot 2H₂O. As an extension of the above mentioned work, [Zn(*IP-2-ac*)₂(H₂O)] (**1**) was prepared using previously described procedure and characterized by single-crystal X-ray diffraction, IR and Raman spectroscopy, thermogravimetric analysis (TG-DTA) and differential scanning calorimetry (DSC) thermal methods. Taking into account pharmaceutical importance of IP scaffold as well as numerous examples of antimicrobial activity of metal-based complexes with structurally similar ligands [12], we also decided to test antimicrobial activity of **1** and previously reported complexes against selected gram-positive and gram-negative bacteria, and *Candida albicans* yeast.

Accordingly, herein, we report structural characterization of unexpected trinuclear [Zn₃(*IP-2-ac*)₆(H₂O)] \cdot 11H₂O (**2**) displaying two different binding modes of *IP-2-ac* anions.

2. Experimental

2.1. General information and materials

Imidazo[1,2-a]pyridin-2-ylacetic acid (*HIP-2-ac*) was synthesized according to previously described procedure [11]. All other reagents were obtained from commercial sources and used without purification. The C, H, and N microanalyses for **1** were carried out on an Elementar vario EL III analyzer.

2.2. Syntheses of **1**, **2**, and **1-a**

Compound 1: [Zn(*IP-2-ac*)₂(H₂O)] was prepared by addition of 25.3 mg (0.085 mmol) of Zn(NO₃)₂ \cdot 6H₂O to 6 mL of water solution containing 30 mg (0.17 mmol) of *HIP-2-ac* and a small quantity of aqueous solution of methylamine (added to adjust the pH to 8).

The resulting solution was inserted into a glass reactor and heated at 100–120 °C for 6–8 h. Colorless crystals of **1** were collected by filtration, washed with cold distilled water, and allowed to dry in air (yield 40%). The same crystals can also be isolated when methylamine is replaced by 25% solution of ammonia (Anal. Calcd for $C_{18}H_{16}N_4O_5Zn$ (%): C, 49.84; H, 3.73; N, 12.92). C, 49.89; H, 3.74; and N, 12.89 were found (%). Compound **1** is poorly soluble in H_2O , DMSO, and other common solvents which hampered the collection of good quality NMR spectra and characterization in solution.

Compound 2: On slow evaporation of filtrate remaining after separation of **1**, small quantities of crystals different from **1** were unexpectedly isolated after ca. three weeks. X-ray single-crystal diffraction analysis revealed that highly hydrated trinuclear $[Zn_3(IP-2-ac)_6(H_2O)] \cdot 11H_2O$, **2** (stable in air for the duration of measurement), was formed. Unfortunately, our attempts to isolate sufficient amount of **2** for further characterization proved unsuccessful. Several crystal growth trials resulted mostly in crystals which decomposed within a few minutes; thus, this material remains unidentified.

Compound 1-a: Crystalline $[Zn(IP-2-ac)_2(D_2O)]$ (deuteration yield > 97%) was obtained by same procedure as **1** with the use of deuterated ligand (recrystallized from D_2O in triplicate), ammonia- d_3 , dehydrated $Zn(NO_3)_2$, and D_2O as solvent.

2.3. X-ray crystallography

Crystallographic measurements were performed on a Kuma KM4-CCD (for **1**) and Xcalibur R (for **2**) automated four-circle diffractometers with graphite monochromated Mo $K\alpha$ radiation at 100(2) K (**1**) or 296(2) K (**2**), using Oxford Cryosystems coolers. Data collection, cell refinement, data reduction, and analysis were carried out with CRYALISCCD and CRYALISRED, respectively [13]. Analytical (for **1**) or multi-scan (for **2**) absorption correction was applied to the data with use of CRYALISRED. Structures were solved with direct methods using SHELXS-2013 [14] and refined by full-matrix least squares with SHELXL-2013 [14] with anisotropic thermal parameters for all non-H atoms, unless otherwise stated below. All hydrogens were initially located in difference Fourier maps (except for disordered ligand anions in **2**, in which they were included from geometry), and in the final refinement cycles were treated as described below. All C-bound hydrogens were placed in calculated positions, with C–H = 0.93–0.99 Å, and refined with a riding model with $U_{iso}(H) = 1.2U_{eq}(C)$. Water hydrogens in **1** were refined freely. In **2**, water hydrogens were refined with $U_{iso}(H) = 1.5U_{eq}(O)$, and with O–H and H···H distances restrained to 0.840(2) and 1.380(2) Å, respectively, and then constrained to ride on their parent atoms (AFIX 3 instruction in SHELXL-2013 [14]). During the refinement of **2**, three of the water molecules were found to be disordered and were refined with O in two positions, each, and with occupancy factors of 0.6 and 0.4 (see the CIF file for details). Moreover, one of the ligand anions was disordered and refined over two locations, with 0.515(19) and 0.485(19) occupancies. In a second ligand anion, the acetate substituent was disordered, and refined over two sites with 0.75(4) and 0.25(4) occupancies. All of the disordered atoms in **2** were refined isotropically. Some restraints on geometry and anisotropic displacement parameters, as well as constraints on the fractional coordinates and ADPs (SAME, SIMU, EXYZ, EADP instructions in SHELXL-2013) were applied in the refinement procedure if appropriate. Selected crystallographic data and structure refinement parameters are summarized in table 1. All figures were made using DIAMOND [15].

Table 1. Summary of crystallographic data and structure refinement for the compounds **1** and **2**.

	Compound 1	Compound 2
CCDC no.	1004864	1020823
Chemical formula	C ₁₈ H ₁₆ N ₄ O ₅ Zn	C ₅₄ H ₆₆ N ₁₂ O ₂₄ Zn ₃
<i>M_r</i>	433.72	1463.29
Crystal system, space group	Monoclinic, <i>C2/c</i>	Monoclinic, <i>P2₁/c</i>
Temperature (K)	100(2)	296(2)
<i>a</i> , <i>b</i> , <i>c</i> (Å)	11.437(3), 9.701(3), 15.976(4)	11.210(4), 33.885(9), 17.596(6)
β (°)	105.41(3)	107.83(3)
<i>V</i> (Å ³)	1708.8(8)	6363(4)
<i>Z</i>	4	4
Radiation type	Mo <i>K</i> α	Mo <i>K</i> α
μ (mm ⁻¹)	1.48	1.21
Crystal size (mm)	0.34 × 0.28 × 0.12	0.20 × 0.08 × 0.08
Absorption correction	Analytical	Multi-scan
<i>T_{min}</i> , <i>T_{max}</i>	0.736, 0.884	0.860, 1.000
No. of measured, independent, and observed [<i>I</i> > 2 σ (<i>I</i>)] reflections	5292, 2069, 1894	67,552, 11,844, 6282
<i>R_{int}</i>	0.026	0.163
(<i>sin</i> θ/λ) _{max} (Å ⁻¹)	0.675	0.606
<i>R</i> [<i>F</i> ² > 2 σ (<i>F</i> ²)], <i>wR</i> (<i>F</i> ²), <i>S</i>	0.031, 0.082, 1.06	0.109, 0.212, 1.06
No. of reflections	2069	11,844
No. of parameters	132	823
Restraints	0	109
$\Delta\rho_{\max}$, $\Delta\rho_{\min}$ (e Å ⁻³)	0.50, -0.30	0.62, -0.54

2.4. Vibrational spectroscopy

ATR-FTIR (attenuated total reflection-infrared) measurements were made using a Bruker Vertex 70v Fourier transform infrared spectrometer equipped with a diamond ATR cell. The spectral data were collected at room temperature from 4000–400 cm⁻¹ to 600–40 cm⁻¹ with a resolution of 4 and 2 cm⁻¹, respectively.

FT-Raman spectra were collected on a Bruker MultiRam spectrometer (Nd:YAG laser with emitting radiation at a wavelength of 1064 nm) equipped with a liquid nitrogen cooled germanium detector. The spectra were accumulated with a resolution of 2 cm⁻¹ and Raman laser power 50 mW.

Instrument control and initial data processing were performed using OPUS software (v. 7.0 Bruker Optics, Ettlingen, Germany).

2.5. Calculations

The normal vibrations of Zn(IP-2-ac)₂(H₂O) were calculated using the GAUSSIAN 09 package [16], employing the B3LYP functional [17] and LanL2DZ basis set [18]. The calculations were performed on the optimized structure, which corresponds well with that determined by single-crystal X-ray diffraction. A noticeable difference was found only for the coordinated water. O–H bond orientations are almost parallel to Zn–O bonds in the calculated structure, whereas a twist is observed in the crystal structure.

Normal vibrations of Zn(IP-2-ac)₂(D₂O) were also computed. Normal vibrations and corresponding IR and Raman bands were characterized on the basis of atom displacement

animation done by the Chemcraft program [19] and potential energy distribution (PED) calculated by Fcart66 package [20]. Theoretical spectra were generated by Chemcraft application, with Lorentzian band shape and 5 cm^{-1} half band width. For easier comparison of observed and calculated band positions, the calculated wavenumbers were scaled by 0.96 factor, typical for applied computation method [21].

2.6. Thermal analysis

TG-DTA was carried out using a Setaram SETSYS 16/18 thermogravimetric analyzer, operating under nitrogen, with a heating rate of 5 °C/min^{-1} from 30 to 500 °C (sample mass 4.312 mg). DSC measurements were performed on a Setaram DSC 92 instrument. Sample (mass 6.0 mg) was contained in an alumina pan in the presence of air as the furnace atmosphere with heating rate of 5 °C/min^{-1} in a temperature range of 30–500 °C.

2.7. Antimicrobial activity studies

The *in vitro* antimicrobial activities of studied ligand and its five complexes with zinc(II), nickel(II), cobalt(II), manganese(II), and cadmium(II) were tested against *Bacillus subtilis*, *Staphylococcus aureus*, *Mycobacterium fortuitum*, *Enterococcus hirae*, *Escherichia coli*, *Pseudomonas aeruginosa*, and *C. albicans*. Bacterial strains were obtained from the Polish Collection of Microorganisms located in the Institute of Immunology and Experimental Therapy of the Polish Academy of Sciences, Wrocław, Poland. Prior to use in tests, the cultures of bacteria were grown on nutrient broth at 37 °C for 24 h.

Antibacterial tests were carried out on solid samples. Compounds under consideration were milled with starch to give an active content of 10%. The resulting powders were pressed using a hydraulic press into 7 mm diameter pellets. Solid pellets were placed on agar plates with inoculated microorganisms and incubated at 37 °C for 24 h, except for *M. fortuitum* for which incubation was carried out for 48 h. After this time, inhibition zones (if present) were measured in mm as $r = (d2 - d1)/2$ (where $d1$ is diameter of pellet and $d2$ is diameter of inhibition zone) and results were documented by digital photography. Pellets containing only starch were used as a control probe and those containing 10% of related M (II) nitrates in starch for comparison. All experiments were performed in duplicate and the average values are presented.

2.8. Electrospray mass spectrometry

ESI-MS experiment for saturated aqueous solution of crystalline solid isolated from post-reaction mixture was performed on a Bruker MicrOTOF-Q spectrometer (Bruker Daltonic, Bremen Germany) equipped with an Apollo II electrospray ionization source with an ion funnel. The spectrum was acquired in a positive ion mode for 50 : 50 (v/v) MeOH/H₂O sample. The instrumental parameters were as follows: the scan range m/z 200–2000, end plate offset -500 V , dry gas nitrogen (4 L/min), temperature 473 K, capillary voltage 4500 V, ion energy 5 eV. Data analysis was carried out with the use of Bruker Daltonics Data Analysis software v. 3.4.

3. Results and discussion

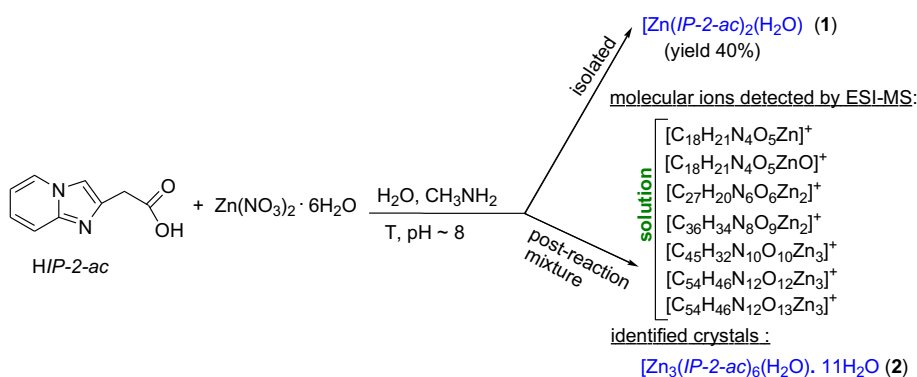
3.1. Preparation of **1** and **2**

As illustrated in scheme 1, $[\text{Zn}(\text{IP-2-ac})_2(\text{H}_2\text{O})]$ (**1**) was prepared using previously reported procedure; however, it was isolated in lower yield as compared to previously synthesized compounds [11]. When filtrate remaining after isolation of **1** was left to stand at room temperature, a few crystals of **2** were unexpectedly and unprecedentedly isolated and one of them was characterized by single-crystal X-ray diffraction.

To understand why our attempts to obtain sufficient amount of **2** were unsuccessful (see experimental part), solid material isolated from post-reaction mixture was dissolved in water and subjected to ESI-MS analysis. ESI-MS is one of the most sensitive and useful techniques providing qualitative information on stoichiometric composition of metal complexes performed in solution [22]. As can be seen in figure S1 (see online supplemental material at <http://dx.doi.org/10.1080/00958972.2015.1048241>), the spectrum exhibits two peaks at $m/z = 437$ and 453 , respectively, attributed to $[\text{Zn}(\text{IP-2-ac})_2(\text{H}_2\text{O})+\text{H}]^+$ and related mononuclear $[\text{C}_{18}\text{H}_{21}\text{N}_4\text{O}_6\text{Zn}]^+$ species. This is confirmed by comparison of experimental and calculated isotope distribution patterns. Lower intensity peaks at m/z 653, 851, 1065, 1247.1, 1265.1 with isotope distribution patterns matching those calculated for $[\text{C}_{27}\text{H}_{20}\text{N}_6\text{O}_6\text{Zn}_2]^+$, $[\text{C}_{36}\text{H}_{34}\text{N}_8\text{O}_9\text{Zn}_2]^+$, $[\text{C}_{45}\text{H}_{32}\text{N}_{10}\text{O}_{10}\text{Zn}_3]^+$, $[\text{C}_{54}\text{H}_{46}\text{N}_{12}\text{O}_{12}\text{Zn}_3]^+$, $[\text{C}_{54}\text{H}_{48}\text{N}_{12}\text{O}_{13}\text{Zn}_3]^+$ were identified. The complicated solution equilibrium involving mononuclear **1** and a variety of multinuclear zinc(II) species suggested by ESI-MS spectrum seems to explain the difficulty in reproducing the crystallization conditions suitable for growing crystals of **2**. Furthermore, these results suggest that solid material isolated from post-reaction mixture may be inhomogeneous. In consequence, only **1** was subjected to further analysis by means of TG-DTA, DSC, and vibrational spectroscopy.

3.2. Molecular structure, crystal packing, and intermolecular interactions in **1**

$[\text{Zn}(\text{IP-2-ac})_2(\text{H}_2\text{O})]$ (**1**) crystallizes in the $C2/c$ space group of the monoclinic crystal system. The molecular structure and atom numbering scheme for **1** are shown in figure 1. Selected geometrical parameters and hydrogen bonds are given in tables 2 and S1 (ESI),



Scheme 1.

respectively. The structure of **1** consists of discrete $\text{Zn}(\text{IP-2-ac})_2(\text{H}_2\text{O})$ coordination entities, in which the zinc(II) is five-coordinate by N1, O1, N1ⁱ, and O1ⁱ from two chelating *IP-2-ac* anions and O1^W from a water molecule. Zinc(II) ion and coordinated O1^W are located on a twofold axis; thus, the asymmetric unit comprises one-half of the complex. Coordination entities are additionally stabilized by C8–H8···O1ⁱ contacts symmetry code: (i) $-x + 1, y, -z + 1/2$; for more details refer to table S1, enabling identification of an intramolecular hydrogen-bonded ring denoted by S(6) graph set notation [23].

The coordination geometries in five-coordinate metal complexes are conveniently described by the Addison parameter defined as $\tau = (\beta - \alpha)/60$ where β and α are the two largest angles in the metal ion coordination sphere. For ideal square-pyramidal (SP) environment, $\beta = \alpha = 180^\circ$ and $\tau = 0.00$, while for perfect trigonal-bipyramidal (TB) environment, $\beta = 180^\circ$ and $\alpha = 120^\circ$ which results in $\tau = 1.00$ [24]. In **1**, the N_2O_3 environment of Zn1 with $\tau = 0.88$ is best described as square-pyramidal distorted TB with almost linear O1–Zn1–O1ⁱ angle ($178.89(7)^\circ$) and O1^W–Zn1–N1ⁱ and N1–Zn1–N1ⁱ angles close to 120° ($116.83(5)^\circ$ and $126.33(9)^\circ$, respectively, table 2). Moreover, the axial Zn–O bonds ($2.078(2) \text{ \AA}$) are somewhat longer than the in-plane Zn–N and Zn–O bonds ($2.043(2)$ and $1.967(2) \text{ \AA}$, respectively). Similar geometries of ZnN_2O_3 environments can also be found in bis(2-aminothiazol-4-yl acetate)(aqua)M(II) complexes ($M = \text{Zn}$ or Cd) [25, 26] as well as i.e. in the zinc(II) complexes with pyridylmethylamide [27], benzimidazole-2-carboxylate [28], or clioquinol [29].

Flexibility of *IP-2-ac* is reflected in an orientation of acetate moiety, as seen by N1–C2–C10–C11 and C2–C10–C11–O1 torsion angles ($-45.4(3)$ and $16.7(3)^\circ$, respectively, table 2). Similar values are also observed in the previously reported $[\text{M}(\text{IP-2-ac})_2(\text{H}_2\text{O})_2 \cdot 2\text{H}_2\text{O}]$ complexes of nickel(II), cobalt(II), manganese(II), and cadmium(II) [11].

In the crystal of **1**, coordinated water molecules interact with the uncoordinated carboxylate oxygen of neighboring $\text{Zn}(\text{IP-2-ac})_2(\text{H}_2\text{O})$ coordination entities by O1^W–H1^W···O2ⁱⁱ hydrogen bonds to form a supramolecular chain that can be denoted by a $\text{C}_4^4(6)$ graph set. Chains are associated into $\text{R}_4^4(22)$ ring motifs, resulting in the formation of a molecular layer in the crystallographic *ab* plane, additionally stabilized by C10–H10^B···O1^{iv} contacts (figure 2). Inter-layer stabilization of the 3-D arrangement in the crystal lattice is provided

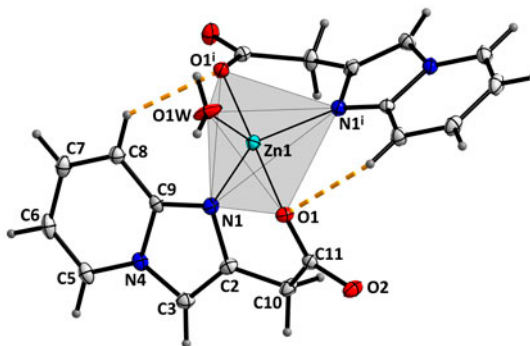


Figure 1. Molecular geometry, thermal ellipsoids (shown at 50% probability), and numbering scheme for $\text{Zn}(\text{IP-2-ac})_2(\text{H}_2\text{O})$ coordination entity in **1**. Hydrogen bonds are indicated by orange dashed lines [symmetry code: (i) $-x + 1, y, -z + 1/2$; for more details refer to table S1] (see <http://dx.doi.org/10.1080/00958972.2015.1048241> for color version).

Table 2. Selected interatomic distances (Å), bond angles (deg), and torsion angles (deg) for the **1** and **2**.

Compound 1		Compound 2	
Bond lengths		Bond lengths	
Zn1–O1 <i>W</i>	1.967(2)	Zn1–O1A	2.140(6)
Zn1–O1, O1 ⁱ	2.078(2)	Zn1–N1A	2.033(7)
Zn1–N1, N1 ⁱ	2.043(2)	Zn1–O1B	2.035(13)
<i>Bond angles</i>		Zn1–N1B	2.027(7)
O1 <i>W</i> –Zn1–O1, O1 ⁱ	89.45(4)	Zn1–O2D	2.004(6)
O1 <i>W</i> –Zn1–N1, N1 ⁱ	116.83(5)	Zn2–O1 <i>W</i>	1.982(6)
O1–Zn1–O1 ⁱ	178.89(7)	Zn2–O1C	2.132(5)
O1–Zn1–N1	86.84(6)	Zn2–N1C	2.028(6)
O1–Zn1–N1 ⁱ	93.66(6)	Zn2–O1D	2.134(6)
N1–Zn1–N1 ⁱ	126.33(9)	Zn2–N1D	2.003(7)
<i>Torsion angles</i>		Zn3–O1F	2.168(6)
N1–C2–C10–C11	–45.4(3)	Zn3–N1F	2.034(7)
C2–C10–C11–O1	16.7(3)	Zn3–O1E	2.130(13)
		Zn3–N1E	2.016(10)
		Zn3–O2C	1.976(6)
		Bond angles	
		O1A–Zn1–O1B	176.6(3)
		O2D–Zn1–N1B	134.4(3)
		N1A–Zn1–N1B	112.5(3)
		O1C–Zn2–O1D	174.2(2)
		O1 <i>W</i> –Zn2–N1C	121.4(3)
		N1C–Zn2–N1D	122.7(3)
		O1E–Zn3–O1F	174.6(5)
		O2C–Zn3–N1E	131.7(5)
		N1E–Zn3–N1F	115.4(6)
		Torsion angles	
		N1A–C2A–C10A–C11A	–53.8(13)
		C2A–C10A–C11A–O1A	36.2(13)
		N1B–C2B–C10B–C11B	–56.6(14)
		C2B–C10B–C11B–O1B	49(2)
		N1C–C2C–C10C–C11C	57.9(11)
		C2C–C10C–C11C–O1C	–47.4(11)
		N1D–C2D–C10D–C11D	51.5(12)
		C2D–C10D–C11D–O1D	–41.5(12)
		N1E–C2E–C10E–C11E	–55.7(16)
		C2E–C10E–C11E–O1E	41(2)
		N1F–C2F–C10F–C11F	–58.5(11)
		C2F–C10F–C11F–O1F	67.8(10)

Symmetry code: (i) $-x+1, y, -z+1/2$.

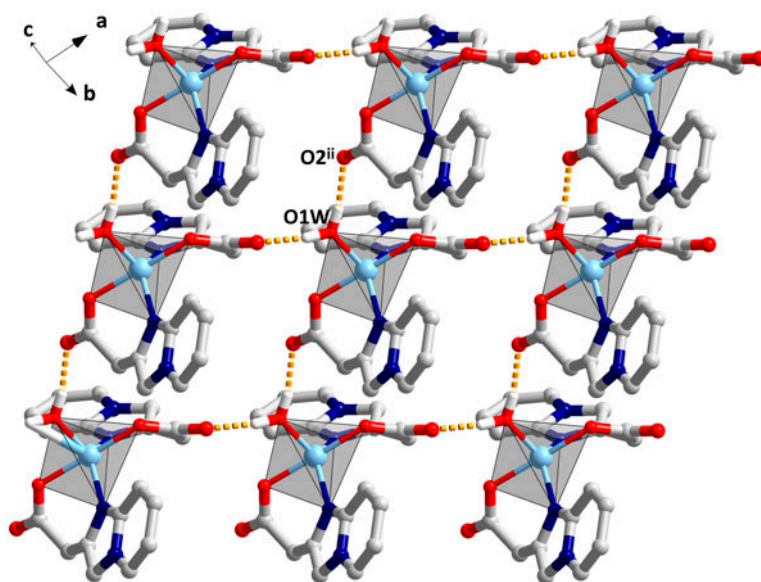


Figure 2. A packing diagram for **1**, showing hydrogen bonds (orange dashed lines) between $\text{Zn}(\text{IP-2-ac})_2(\text{H}_2\text{O})$ coordination entities, leading to the formation of a 2-D network in the crystallographic ab plane. C-bound hydrogens were omitted for clarity (symmetry code: (ii) $-x + 3/2, y - 1/2, -z + 1/2$; for more details refer to table S1) (see <http://dx.doi.org/10.1080/00958972.2015.1048241> for color version).

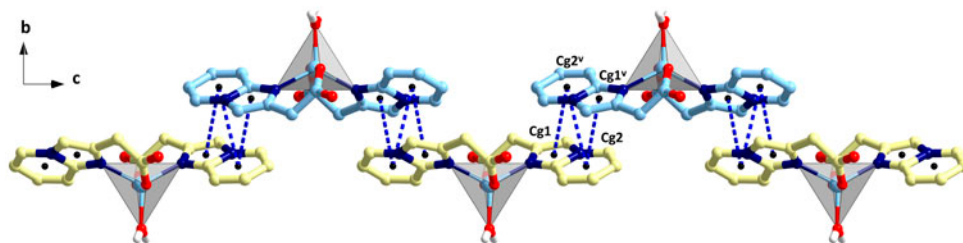


Figure 3. A packing diagram for **1**, showing $\pi \cdots \pi$ interactions (blue dashed lines) between $\text{Zn}(\text{IP-2-ac})_2(\text{H}_2\text{O})$ coordination entities in neighboring layers (constituents are shown in blue and yellow). C-bound hydrogens were omitted for clarity (symmetry code: (v) $-x + 1, -y + 1, -z + 1$; for more details refer to table S1) (see <http://dx.doi.org/10.1080/00958972.2015.1048241> for color version).

by $\text{C7-H7} \cdots \text{O2}^{\text{iii}}$ contacts as well as $\pi \cdots \pi$ interactions, with the latter presented in figure 3 (geometrical parameters in table S1).

3.3. Molecular structure, crystal packing, and intermolecular interactions in **2**

$[\text{Zn}_3(\text{IP-2-ac})_6(\text{H}_2\text{O})] \cdot 11\text{H}_2\text{O}$ (**2**) crystallizes in the $P2_1/c$ space group of the monoclinic crystal system. The molecular structure and atom numbering scheme for **2** are shown in figures 4 and S2. Atoms of disordered ligands and water molecules refined with minor occupancies (see Section 2 for further details) were omitted for clarity in both figures and

discussion. Selected geometrical parameters and hydrogen bonds are given in tables 2 and S1, respectively.

The structure of **2** consists of discrete trinuclear $Zn_3(IP-2-ac)_6(H_2O)$ coordination entities, surrounded by multiple water molecules. The arrangement of zinc(II) ions is close to collinear ($Zn1 \cdots Zn2 \cdots Zn3$ angle of $168.9(1)^\circ$), whereas the $Zn1 \cdots Zn2$, $Zn2 \cdots Zn3$ distances are $4.938(2)$ and $4.975(2)$ Å, respectively. All three zinc(II) ions exhibit a five-coordinate ZnN_2O_3 geometry. The coordination environment of $Zn2$ ion is built up by N1 and O1 from two chelated *IP-2-ac* anions and an *O1W* from water. For the terminal $Zn1$ and $Zn3$ ions (see figure 4), the coordination environment is created by N1 and O1 from two chelated *IP-2-ac* anions and non-coordinating O2 provided by carboxylate of ligand chelating $Zn2$. A similar trinuclear $[ZnN_2O_3]_3$ coordination entity formed by zinc(II) and phenoxido/alkoxido mixed ligands has been reported previously [30].

As described above, the N1–C2–C10–C11 and C2–C10–C11–O1 torsion angles describe the conformation of *IP-2-ac* anions. The corresponding values for *IP-2-ac* chelating terminal $Zn1$ and $Zn3$ in **2** exhibit similar conformations to that present in **1** and previously reported complexes [11], whereas the bridging *IP-2-ac* anions adopt opposite orientations of the acetate group as related to the ligand backbone (table 2). An additional stabilization of **2** is provided by C–H \cdots O-type contacts and $\pi \cdots \pi$ interactions (table S1).

The ZnN_2O_3 coordination environments in **2** are best described by a distorted TB geometry with corresponding angles and bond lengths similar to those in **1** (table 2). The environment around $Zn2$ is very similar to $Zn1$ of **1** with a τ value of 0.86 [24]. For $Zn1$ and $Zn3$, the τ values equal 0.70 and 0.72, respectively, indicating larger deviation toward square pyramid as compared to $Zn2$. This suggests that $Zn(IP-2-ac)_2(H_2O)$ may be regarded as a precursor in the formation of $Zn_3(IP-2-ac)_6(H_2O)$. A possible path for trinuclear entity formation deduced based on ESI-MS spectrum (figure S1) is given in figure S3.

In the crystal structure of **2**, neighboring $Zn_3(IP-2-ac)_6(H_2O)$ coordination entities interact through an array of O–H \cdots O hydrogen bonds formed between lattice water

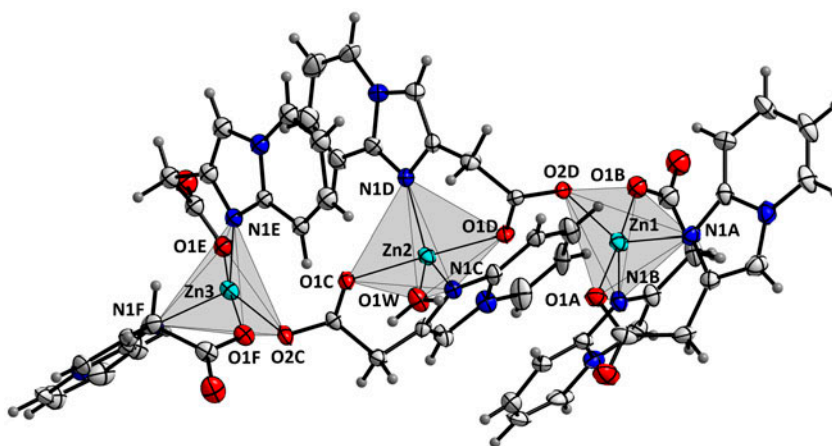


Figure 4. Molecular geometry, thermal ellipsoids (shown at 20% probability level), and partial numbering scheme for $Zn_3(IP-2-ac)_6(H_2O)$ in **2**. C-bound hydrogens and ligand atoms refined with minor occupancies were omitted for clarity. For omitted species and numbering schemes of ligand backbones, refer to figure S2.

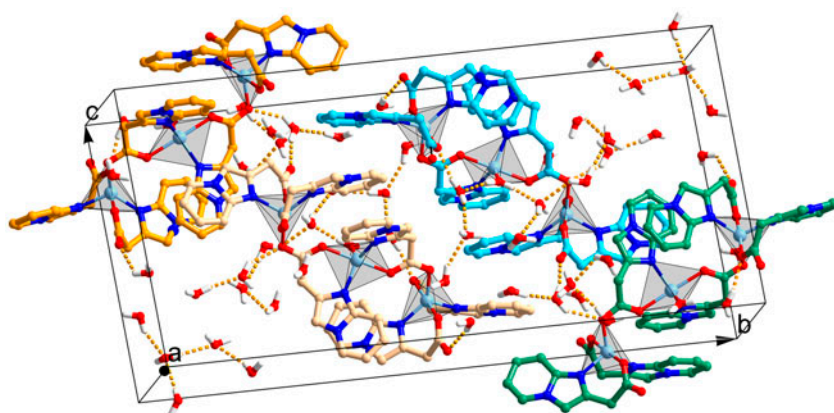


Figure 5. Packing of molecules in the unit cell of **2**, showing four $Zn_3(IP-2-ac)_6(H_2O)$ coordination entities (orange, tan, blue, and green) along with water molecules and O–H \cdots O hydrogen bonds (orange dashed lines) (see <http://dx.doi.org/10.1080/00958972.2015.1048241> for color version).

molecules, $O1W$ coordinated water, and carboxylate groups of *IP-2-ac* (table S1), resulting in a 3-D network. The 3-D crystal lattice is additionally stabilized by C–H \cdots O contacts and $\pi\cdots\pi$ interactions (not shown herein, see table S1 for geometrical details). Packing in the unit cell of **2** is shown in figure 5.

3.4. Thermal stability of **1**

Thermal behavior of **1** was assessed on crystalline samples by means of TG-DTA and DSC analyses carried out under nitrogen and air, respectively. There is no lattice water in the crystal of **1**; therefore, its thermal stability was higher compared to previously reported $[M(IP-2-ac)_2(H_2O)_2]\cdot 2H_2O$ ($M = Co, Ni, Mn, Cd$) complexes, all of which decompose below 100 °C [11]. Thermogram of **1** (figure S4) shows two steps of decomposition from 30–500 °C. The first entropy-driven weight loss takes place above 139 °C and corresponds to release of ca. one mole of coordinated water per mole of zinc (exp. 3.6%, calcd. 4.1%). Thereafter, subsequent endothermic event occurs (onset temperature 323 °C, 48.6% weight loss) which can be attributed to decomposition of **1** by gradual elimination of coordinated ligands due to breaking coordination bonds. The DSC curve exhibits roughly similar endothermic event corresponding to dehydration of **1** (onset temperature 145 °C, $\Delta H = 116.84$ J/g, figure S5); however, further sample heating in oxidizing atmosphere leads to exothermic processes above 310 °C (onset temperature 313 °C, $\Delta H = -393$ J/g). Similar behavior was observed for $[M(IP-2-ac)_2(H_2O)_2]\cdot 2H_2O$ ($M = Co, Ni, Mn, Cd$) complexes and attributed to simultaneous release of ligands and their thermal decomposition [11].

3.5. Vibrational analysis of **1**

The presence of water molecule in the structure of **1** suggested the application of H/D isotope substitution for experimental detection of bands related to H_2O and H_2O-Zn vibrations. From the respective spectra shown in figure 6, deuteration caused much more spectral changes than expected. Apart from typical effects in the spectral region above 1800 cm^{-1} ,

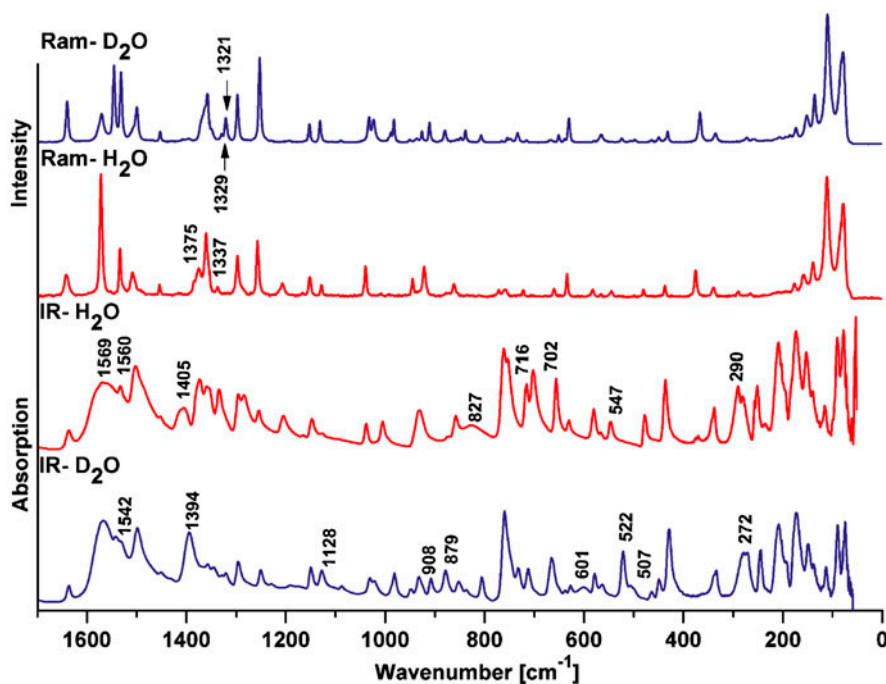


Figure 6. Experimental Raman and IR spectra of crystalline **1** and its deuterated $[\text{Zn}(\text{IP-2-ac})_2(\text{D}_2\text{O})]$ (**1-a**) analog.

several differences between spectra of parent $[\text{Zn}(\text{IP-2-ac})_2(\text{H}_2\text{O})]$ (**1**) and deuterated $[\text{Zn}(\text{IP-2-ac})_2(\text{D}_2\text{O})]$ (**1-a**) complexes are observed between 1800 and 400 cm^{-1} . Among 30 IR bands recorded [figure 6], nine bands significantly change position or intensity. Such influence of $\text{H}_2\text{O}/\text{D}_2\text{O}$ substitution on molecular dynamics suggests that H_2O group motions strongly couple with other internal vibrations. Coupling is also expected between pyridine and imidazole ring vibrations as both rings have two common atoms. In order to assign the spectra as accurately as possible, DFT calculations were performed, which also included the deuteration effects. However, the results of calculations should be treated with caution because the computed molecular model does not fully reflect the environment of water ligand involved in intermolecular hydrogen bonds (figure 2 and table S1). In theoretical attempt, water molecule is considered to act as proton donor in the $\text{O}_{42}-\text{H}_{44}\cdots\text{O}_{33}$ intramolecular interaction (refer to figure S6 for atom numbering). In consequence, the calculated results were used mostly for skeletal and C–H group vibration assignments, whereas in the characterization of water-related bands, deuteration effects and literature data were applied first.

The results of such approach are reflected in table 3 presenting measured and calculated data together with proposed assignments. In order to minimize the size of table 3, the vibrations related to six-membered aromatic ring skeleton and C–H groups were omitted. These data can be found in supplementary table S2. Also, in the presentation of computed data, the theoretical band positions are given instead of normal vibration wavenumbers. Most of the calculated bands are generated by two normal modes of close wavenumbers and related to similar vibrations in two ligands present in the $[\text{Zn}(\text{IP-2-ac})_2(\text{H}_2\text{O})]$ complex. For that

Table 3. Selection of observed and calculated IR and Raman bands [cm^{-1}] attributed to vibrations of $[\text{Zn}(\text{IP-2-ac})_2(\text{H}_2\text{O})]$ (**1**) with their general and PED-based assignments. (Atom numbering scheme is consistent with that provided in figure S6.)

Nb.	Observed ^a				Calculated – 0.96 scaled				General assignment ^{b,c}	PED ^d (mostly $\geq 10\%$)
	H_2O		D_2O		H_2O		D_2O			
	IR	Raman	IR	Raman	IR int. R int]	D ₂ O [IR int. R int]				
1	1569br	1572vs	1567s	1571m	1526[97, 292]	1527 [90, 293]	$\nu(\text{C}-\text{C})_{\text{im}}$	$\nu(\text{C}_2-\text{C}_3)-34 + \nu(\text{C}_{10}-\text{C}_2)-13$		
2	1560sh	n.o.	1542s	1546s	1586 [930, 22]	1579 [1018, 23]	$\nu(\text{C}=\text{O})$	$\nu(\text{C}_{11}-\text{O}_{13})-69$		
3	1560sh	n.o.	1128m	1131w	1425 [192, 15]	1050 [176, 7]	$\delta(\text{H}_2\text{O})/\delta(\text{D}_2\text{O})$	$\delta(\text{H}_{43}-\text{O}_{42}-\text{H}_{44})-35/44$		
4	1405m	n.o.	1394s	1395w	1424 [4, 28]	1423 [2, 5]	$\nu(\text{C}-\text{N})_{\text{py}}$	$\nu(\text{N}_4-\text{C}_2)-12 + \delta(\text{H}_{29}-\text{O}_{27}-\text{H}_{44})-5$		
5	1373s	1375 m	1321m	1321 m	1346[66, 223]	1344 [65, 223]	$\nu(\text{C}-\text{N})_{\text{py}}$	$\nu(\text{N}_4-\text{C}_2)-13 + \nu(\text{N}_4-\text{C}_9)-7$		
6	1359s	1360s	1357m	1358s	1326 [21, 27]	1326 [21, 25]	$\nu_2(\text{N}-\text{C})$	$\nu(\text{N}_1-\text{C}_9)-6$		
7	1334m	1337w	1329m	1329m	1313 [95, 22]	1313 [90, 23]	$\nu_2(\text{N}-\text{C})_{\text{im}}$	$\nu(\text{N}_1-\text{C}_2)-14 + \nu(\text{N}_1-\text{C}_9)-11$		
8	1295s	1297s	1296s	1297s	1270 [137, 63]	1270 [191, 81]	$\nu_2(\text{C}-\text{N})_{\text{im}}$	$\nu(\text{N}_1-\text{C}_9)-6$		
9	1284s	n.o.	1296s	1297s	1226 [426, 16]	1227 [373, 134]	$\nu(\text{C}-\text{O}) + \delta(\text{H}_2\text{O})/\nu(\text{C}-\text{O})$	$\nu(\text{C}_{11}-\text{O}_{12})-32 + \nu(\text{C}_{10}-\text{C}_{11})-15$		
10	1254m	1257s	1250m	1253s	1219 [156, 143]	1219 [127, 138]	$\nu(\text{C}-\text{N})$	$\nu(\text{C}_3-\text{N}_4)-19$		
11			908m	911m			O–D...O deformation			
12			879m	880m			O–D...O deformation			
13	858m	862m	852w	848w	830 [17, 38]	830 [16, 38]	$\nu(\text{N}-\text{C})$	$\nu(\text{N}_4-\text{C}_9)-10$		
14	827m,br	n.o.	601w,br	n.o.			$\rho_1(\text{H}_2\text{O})/\rho_1(\text{D}_2\text{O})$			
15	716s	722w	522s	524w			$\rho_1(\text{H}_2\text{O})/\rho_1(\text{D}_2\text{O})$			
	702s		507m							
16	656s	660w	665m	668vw	669 [54, 9]	665 [53, 9]	$\delta(\text{C}=\text{O})$	$\delta(\text{O}_{12}-\text{C}_{11}-\text{O}_{13})-10$		
17	547m	545m	450m	450m			$\rho_w(\text{H}_2\text{O})/\rho_w(\text{D}_2\text{O})$			
18	479w	480w	464w	464w	469 [2, 4]	468 [5, 9]	$\delta(\text{py-im})$	$\delta(\text{N}_1-\text{C}_9-\text{C}_8)-12 - \delta(\text{C}_3-\text{N}_4-\text{C}_2)-10$		
19	370vw	376m	n.o.	367m	370 [7, 16]	370 [7, 16]	$\delta(\text{C}-\text{C}=\text{O})$	$\delta(\text{C}_{10}-\text{C}_{11}-\text{O}_{13})-18 - \delta(\text{C}_{10}-\text{C}_{11}-\text{O}_{12})-12$		
20	338m	340w	334m	335w	340 [7, 14]	339 [6, 11]	$\nu(\text{Zn}-\text{O})$	$\nu(\text{Zn}_{14}-\text{O}_{12})-14$		
21	298s	289w	272s	272w	329 [2, 8]	318 [1, 7]	$\nu(\text{Zn}-\text{OH}_2) / \nu(\text{Zn}-\text{OD}_2)$	$\nu(\text{Zn}_{14}-\text{O}_{12})-28 / \nu(\text{Zn}_{14}-\text{O}_{42})-40$		
22	281s	n.o.	278s	n.o.	389 [4, 29]	288 [5, 24]	$\nu(\text{Zn}-\text{O})$	$\nu(\text{Zn}_{14}-\text{O}_{12})-35$		
23	257m	n.o.	245s	n.o.	272 [7, 10]	272 [8, 20]	$\nu(\text{Zn}-\text{N})$	$\nu(\text{Zn}_{14}-\text{N}_2)-17$		
	251s				263 [1, 18]	262 [1, 25]		$\nu(\text{Zn}_{14}-\text{N}_1)-16$		
24	209s	n.o.	208s	n.o.	217 [5, 26]	213 [5, 26]	$\nu(\text{Zn}-\text{O}) + \nu(\text{C}-\text{O}-\text{Zn}-\text{O})$	$\nu(\text{Zn}_{14}-\text{O}_{13})-11 + \nu(\text{Zn}_{14}-\text{O}_{12})-10 + \nu(\text{C}_{32}-\text{O}_{33}-\text{Zn}_{14}-\text{O}_{12})$		
25	173s	176w	173s	174w	178 [7, 20]	181 [3, 10]	$\nu(\text{O}-\text{Zn}-\text{O}-\text{C}) + \nu(\text{Zn}-\text{N})$	$\nu(\text{O}_{33}-\text{Zn}_{14}-\text{O}_{12}-\text{C}_{11})-36 + \nu(\text{Zn}_{14}-\text{N})-24$		
26	153s	157m	150m	152m	155 [4, 7]	153 [9, 18]	$\nu(\text{Zn}-\text{O}-\text{C}) + \nu(\text{C}-\text{O}-\text{Zn}-\text{O})$	$\nu(\text{Zn}_{14}-\text{O}_{12}-\text{C}_{11}-\text{O}_{13})-57 + \nu(\text{C}_{32}-\text{O}_{33}-\text{Zn}_{14}-\text{O}_{12})-27$		
27	140w	139m	139w	136m	133 [4, 16]	128 [4, 17]	$\nu(\text{Zn}-\text{O}-\text{C}) + \nu(\text{O}-\text{Zn}-\text{O}-\text{C})$	$\nu(\text{Zn}_{14}-\text{O}_{12}-\text{C}_{11}-\text{O}_{13})-30 + \nu(\text{O}_{32}-\text{Zn}_{14}-\text{O}_{12}-\text{C}_{11})-28$		
28	116 m	112s	113m	110s	101 [7, 12]	100 [6, 12]	$\nu(\text{C}-\text{C}-\text{C}-\text{N}) + \nu(\text{Zn}-\text{N})$	$\nu(\text{C}_{11}-\text{C}_{10}-\text{C}_2-\text{N}_1)-13 + \nu(\text{Zn}_{14}-\text{N}_1)-12$		
29	91s	n.o.	90	n.o.			Lattice			
30	78s	79s	75s	79s			Lattice			

^as – strong, m – medium, w – weak, vs – very strong, vw – very weak, sh – shoulder, br – broad, n.o. – not observed.

^b ν_{as} – antisymmetric stretching, ν_s – symmetric stretching, δ – bending in-plane, δ – bending out-of-plane, γ – torsion.

^cThe slash separates the assignment for parent and deuterated compound.

^dIn case of ligand modes very similar in both ligand molecules, the PED data are given only for one ligand.

reason, also the PED terms for only one ligand are given – the omitted ones, which usually are of similar values, can be amended using figure S6.

The bending vibration of water molecule was assigned to the 1560 cm^{-1} strong shoulder of intense 1569 cm^{-1} IR band, together with $\nu(\text{C}=\text{O})$ mode. This shoulder has no counterpart in the Raman spectrum, which is consistent with the spectroscopic criterion of bond polarity. After deuteration, the $\nu(\text{C}=\text{O})$ vibration shifts to 1542 cm^{-1} while the $\delta(\text{D}_2\text{O})$ was attributed to band at 1128 cm^{-1} , which intensity significantly increases upon deuteration. This band was proposed based on $\delta(\text{H}_2\text{O})/\delta(\text{D}_2\text{O})$ ratio which in the theoretical spectra is 1.36. Next, band sensitive to $\text{H}_2\text{O}/\text{D}_2\text{O}$ substitution is observed at 1405 cm^{-1} (1394 cm^{-1} for deuterated complex). This band was assigned to calculated 1424 cm^{-1} mode with significant $\text{C}-\text{N}_{\text{py}}$ bond stretching, but also with small contribution of water bending vibration causing the mentioned isotope shift. Similar coupling with $\delta(\text{H}_2\text{O})$ (not reflected in calculations) probably causes the deuteration effects in the $1440\text{--}1300\text{ cm}^{-1}$ region, where respective changes are seen in the Raman spectra more clearly than in the IR ones. Taking into account the relative intensities, medium intensity Raman band at 1375 cm^{-1} shifts to 1321 cm^{-1} upon deuteration, whereas weak band at 1337 cm^{-1} appears as shoulder at 1329 cm^{-1} . Both vibrations show significant contributions of $\nu(\text{C}-\text{N})$ modes in pyridine and imidazole rings, respectively.

The deformation modes (rocking, twisting, and wagging) of bonded water are usually strongly changed by hydrogen bonding; therefore, their assignment cannot be directly related to respective calculated modes. These vibrations were attributed to bands at 827 (rocking), 716 , 702 (twisting), and 547 cm^{-1} (wagging) based on literature data [31, 32]. In metal complexes, the vibrations of central atom are most interesting. Based on “classical” approach to metal–ligand vibrations, one should expect pairs of antisymmetric and symmetric $\text{Zn}-\text{O}$ and $\text{Zn}-\text{N}$ vibrations plus one vibration consisting in $\text{Zn}-\text{OH}_2$ bond stretching. The last vibration should be distinguished by deuteration downshift caused by heavier mass of D_2O molecule. The calculations predicted such shift as 11 cm^{-1} for vibration at 343 cm^{-1} . Inspection of $350\text{--}250\text{ cm}^{-1}$ IR region revealed the 290 cm^{-1} band as the most sensitive to deuteration (18 cm^{-1} downshift if 272 cm^{-1} band is taken as the $\nu(\text{Zn}-\text{OD}_2)$ counterpart). Thus, the 290 cm^{-1} band was assigned to the 343 cm^{-1} vibration having the greatest PED contribution of $\text{Zn}-\text{OH}_2$ stretching vibration. As results from PED analysis and normal mode visualizations, the remaining metal–ligand stretching vibrations do not couple and not form the antisymmetric and symmetric motions. The $\text{Zn}-\text{L}$ vibrations between 350 and 100 cm^{-1} (table 3) contribute in several normal modes frequently together with torsion vibrations in which the central metal is involved.

3.6. Antimicrobial screening of $[\text{Zn}(\text{IP-2-ac})_2(\text{H}_2\text{O})]$ (1): a comparison with $[\text{M}(\text{IP-2-ac})_2(\text{H}_2\text{O})_2]\cdot 2\text{H}_2\text{O}$ ($\text{M} = \text{Co}, \text{Ni}, \text{Mn}, \text{Cd}$) complexes

Compound **1**, metal-free *HIP-2-ac* and previously described crystalline $[\text{M}(\text{IP-2-ac})_2(\text{H}_2\text{O})_2]\cdot 2\text{H}_2\text{O}$ complexes [11] were screened for their effect on microorganisms. The inhibition zones of microbial growth for ligand, **1**, and starch used as a control probe are summarized in figure 7. Figure S7 presents analogous data for $[\text{M}(\text{IP-2-ac})_2(\text{H}_2\text{O})_2]\cdot 2\text{H}_2\text{O}$ complexes, and related photos are collected in table S3.

Free ligand did not exhibit antimicrobial activity against the tested species. The nitrate salts were active against almost all species suggesting profound role of metal ions in inhibition of microbial species growth. Among five metal complexes studied, the best results

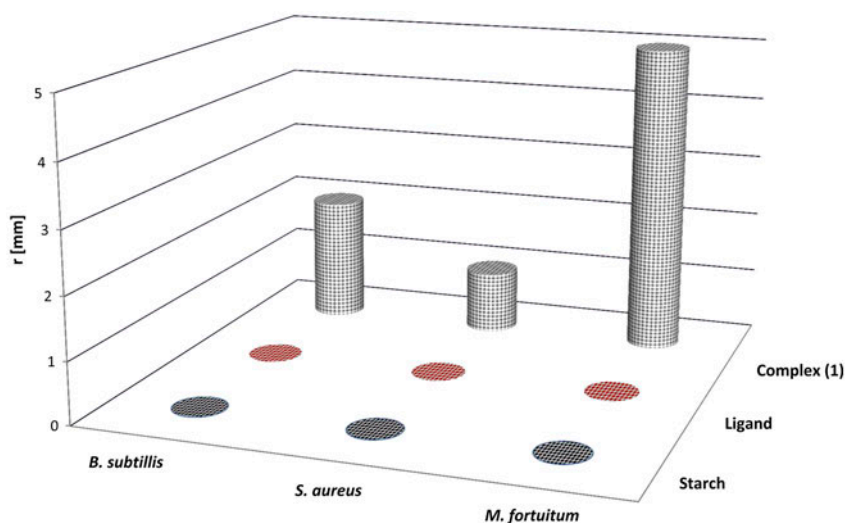


Figure 7. Effect of **1** (10% of active content in starch) on *B. subtilis*, *S. aureus*, and *M. fortuitum* growth expressed as $r = (d_2 - d_1)/2$ (d_1 – diameter of pellet, d_2 – diameter of inhibition zone).

were obtained for **1** and $[\text{Cd}(\text{IP-2-ac})_2(\text{H}_2\text{O})_2] \cdot 2\text{H}_2\text{O}$, whereas related nickel(II), cobalt(II), and manganese(II) complexes were inactive under conditions of the experiment. Chelation of zinc(II) and cadmium(II) ions by *IP-2-ac* diminished effectiveness of inhibition of bacterial growth as compared to related nitrate salts (figure S7). This can be explained as a result of slow dissociation of coordination compounds in the test environment, and consequent decrease in bioavailability of both cations as compared to simple salts.

All microbial species except for *S. aureus* and *P. aeruginosa* were susceptible when exposed to $[\text{Cd}(\text{IP-2-ac})_2(\text{H}_2\text{O})_2] \cdot 2\text{H}_2\text{O}$ (figure S7), whereas $[\text{Zn}(\text{IP-2-ac})_2(\text{H}_2\text{O})]$ exhibited inhibitory activity only against *M. fortuitum*, *B. subtilis*, and *S. aureus* (figure 7). Antimicrobial activity of cadmium complex against most of the tested species is not surprising because of well documented toxicity of this element [33]. On the other hand, $[\text{Zn}(\text{IP-2-ac})_2(\text{H}_2\text{O})]$ (**1**) and $[\text{Cd}(\text{IP-2-ac})_2(\text{H}_2\text{O})_2] \cdot 2\text{H}_2\text{O}$ demonstrated similar antibacterial activities against *M. fortuitum*, and the former complex was the only inhibitor of *S. aureus* growth. Taken together, these results suggest dependence of inhibitory activity of **1** on bacterial cell wall composition (only gram-positive bacteria are susceptible for the treatment) and point to profound role of Zn(II) in inhibition of *S. aureus* metabolism [34].

4. Conclusion

The reaction of *HIP-2-ac* with zinc(II) nitrate carried out under slightly alkaline conditions afforded two crystalline complexes, $[\text{Zn}(\text{IP-2-ac})_2(\text{H}_2\text{O})]$ (**1**) obtained as the main product and $[\text{Zn}_3(\text{IP-2-ac})_6(\text{H}_2\text{O})] \cdot 11\text{H}_2\text{O}$ (**2**).

In both **1** and **2**, the zinc(II) ions are five-coordinate with N_2O_3 coordination environment best described as distorted TB. In **1**, *IP-2-ac* anions are coordinated through *N,O* donors. In **2**, both bidentate and μ -bridging binding modes are observed. The crystal of **1** comprises

discrete $\text{Zn}(\text{IP-2-ac})_2(\text{H}_2\text{O})$ coordination entities combined into layers by hydrogen bonds formed between coordinated water molecules and carboxylate moieties. Inter-layer stabilization of the 3-D crystal lattice is provided by weak $\text{C-H}\cdots\text{O}$ contacts and $\pi\cdots\pi$ interactions. The structure of **2** consists of discrete trinuclear $\text{Zn}_3(\text{IP-2-ac})_6(\text{H}_2\text{O})$ coordination entities, combined into a 3-D hydrogen-bonded network by multiple water molecules.

Based on DFT calculations and deuteration effects, vibrational assignments of IR and Raman spectra of **1** were done. Special attention was paid to water-related vibrations monitored by $\text{H}_2\text{O}/\text{D}_2\text{O}$ substitution. Furthermore, TG-DTA and DSC experiments revealed higher thermal stability of **1** (up to 139 °C) as compared to previously studied $[\text{M}(\text{IP-2-ac})_2(\text{H}_2\text{O})_2]\cdot 2\text{H}_2\text{O}$ complexes of cobalt(II), nickel(II), manganese(II), and cadmium(II).

Screening for antimicrobial activity of **1** and $[\text{M}(\text{IP-2-ac})_2(\text{H}_2\text{O})_2]\cdot 2\text{H}_2\text{O}$ (M = Co, Ni, Mn, Cd) revealed that most microbial species are susceptible when exposed to $[\text{Cd}(\text{IP-2-ac})_2(\text{H}_2\text{O})_2]\cdot 2\text{H}_2\text{O}$, whereas **1** inhibits growth of gram-positive bacteria such as *M. fortuitum*, *B. subtilis*, and *S. aureus*. Furthermore, **1** is the only complex active against *S. aureus*, which points to profound role of zinc(II) in the inhibition of *S. aureus* metabolism.

Supplementary material

CCDC No. 1004864 (**1**) and 1020823 (**2**) contain the supplementary crystallographic data for this article. These data can be obtained free of charge via www.ccdc.cam.ac.uk, or from the Cambridge Crystallographic Data Center, 12 Union Road, Cambridge CB2 1EZ, UK; fax: (+44) 1223 336 033; or e-mail: deposit@ccdc.cam.ac.uk.

Disclosure statement

No potential conflict of interest was reported by the authors.

Funding

This work was supported by a statutory activity subsidy from the Polish Ministry of Science and Higher Education for the Department of Chemistry of Wrocław University of Technology. We also gratefully acknowledge the instrumental grant 6221/IA/119/2012 from Polish Ministry of Science and Higher Education, which supported our Integrated Laboratory of Research and Engineering of Advanced Materials where IR measurements were performed and Wrocław Center of Networking and Supercomputing for the generous allotment of computer time.

References

- [1] C. Hulme, Y.-S. Lee. *Mol. Divers.*, **12**, 1 (2008).
- [2] C. Enguehard-Gueiffier, A. Gueiffier. *Mini-Rev. Med. Chem.*, **7**, 888 (2007).
- [3] (a) G. Yong, Y. Li, W. She, Y. Zhang. *Chem. Eur. J.*, **17**, 12495 (2011); (b) G.-P. Yong, Y.-Z. Li, C.-F. Li, Y.-M. Zhang, W.-L. She. *Dalton Trans.*, **40**, 4131 (2011); (c) G.-P. Yong, Y.-Z. Li, Y.-M. Zhang, W.-L. She. *Cryst. Eng. Comm.*, **14**, 1439 (2012).
- [4] G.-P. Yong, S. Qiao, Z.-Y. Wang. *Cryst. Growth Des.*, **8**, 1465 (2008).
- [5] (a) T. Swainston Harrison, G.M. Keating. *CNS Drugs*, **19**, 65 (2005); (b) D.R. Vega, R. Baggio, M. Roca, D. Tombari. *J. Pharm. Sci.*, **100**, 1377 (2011).
- [6] A. Berson, V. Descatoire, A. Sutton, D. Fau, B. Maulny, N. Vadrot, G. Feldmann, B. Berthon, T. Tordjmann, D. Pessayre. *J. Pharmacol. Exp. Ther.*, **299**, 793 (2001).
- [7] K. Mizushige, T. Ueda, K. Yukiiri, H. Suzuki. *Cardiovasc. Drugs Rev.*, **20**, 163 (2002).
- [8] M. Takeuchi, S. Sakamoto, K. Kawamuki, H. Kurihara, H. Nakahara, Y. Isomura. *Chem. Pharm. Bull.*, **46**, 1703 (1998).

- [9] (a) T.H. Al-Tel, R.A. Al-Qawasmeh. *Eur. J. Med. Chem.*, **45**, 5848 (2010); (b) T.H. Al-Tel, R.A. Al-Qawasmeh, R. Zaarour. *Eur. J. Med. Chem.*, **46**, 1874 (2011); (c) N.C. Desai, M.R. Pandya, K.M. Rajpara, V.V. Joshi, H.V. Vaghani, H.M. Satodiya. *Med. Chem. Res.*, **21**, 4437 (2012).
- [10] (a) R. Agrawal, V. Goyal, R. Gupta, R. Pallepogu, R. Kotikalapudi, P.G. Jones, R.K. Bansal. *Polyhedron*, **70**, 138 (2014); (b) G. Song, X. Li. *Organometallics*, **27**, 1936 (2008).
- [11] A. Dylong, M. Sowa, W. Goldman, K. Slepokura, M. Duczmal, A. Wojciechowska, E. Matczak-Jon. *Polyhedron*, **75**, 9 (2014).
- [12] (a) H. López-Sandoval, M.E. Londoño-Lemos, R. Garza-Velasco, I. Poblano-Meléndez, P. Granada-Macias, I. Gracia-Mora, N. Barba-Behrens. *J. Inorg. Biochem.*, **102**, 1267 (2008); (b) O. Sanchez-Guadarrama, H. Lopez-Sandoval, F. Sanchez-Bartez, I. Gracia-Mora, H. Hopfl, N. Barba-Behrens. *J. Inorg. Biochem.*, **103**, 1204 (2009); (c) C.-Y. Guo, Y.-Yu. Wang, K.-Z. Xu, H.-L. Zhu, P. Liu, Q.-Z. Shi, S.-M. Peng. *Polyhedron*, **27**, 3529 (2008); (d) U. Kalinowska-Lis, E.M. Szewczyk, L. Chęcińska, J.M. Wojciechowski, W.M. Wolf, J. Ochocki. *Chem. Med. Chem.*, **9**, 169 (2014).
- [13] Oxford Diffraction. *CrysAlisCCD and CrysAlisRED in Xcalibur R and Kuma KM4-CCD Software*, Oxford Diffraction Ltd, Yarnton, Oxfordshire, England (2009).
- [14] G.M. Sheldrick. *Acta Crystallogr. A*, **64**, 112 (2008).
- [15] K. Brandenburg. *DIAMOND*, Crystal Impact GbR, Bonn, Germany (2005).
- [16] M.J. Frisch, G.W. Trucks, H.B. Schlegel, G.E. Scuseria, M.A. Robb, J.R. Cheeseman, G. Scalmani, V. Barone, B. Mennucci, G.A. Petersson, H. Nakatsuji, M. Caricato, X. Li, H.P. Hratchian, A.F. Izmaylov, J. Bloino, G. Zheng, J.L. Sonnenberg, M. Hada, M. Ehara, K. Toyota, R. Fukuda, J. Hasegawa, M. Ishida, T. Nakajima, Y. Honda, O. Kitao, H. Nakai, T. Vreven, J.A. Montgomery Jr., J.E. Peralta, F. Ogliaro, M. Bearpark, J.J. Heyd, E. Brothers, K.N. Kudin, V.N. Staroverov, T. Keith, R. Kobayashi, J. Normand, K. Raghavachari, A. Rendell, J.C. Burant, S.S. Iyengar, J. Tomasi, M. Cossi, N. Rega, J.M. Millam, M. Klene, J.E. Knox, J.B. Cross, V. Bakken, C. Adamo, J. Jaramillo, R. Gomperts, R.E. Stratmann, O. Yazyev, A.J. Austin, R. Cammi, C. Pomelli, J.W. Ochterski, R.L. Martin, K. Morokuma, V.G. Zakrzewski, G.A. Voth, P. Salvador, J.J. Dannenberg, S. Dapprich, A.D. Daniels, O. Farkas, J.B. Foresman, J.V. Ortiz, J. Cioslowski, D.J. Fox. *Gaussian 09, Revision D.01*, Gaussian, Inc., Wallingford, CT (2013).
- [17] A.D. Becke. *J. Chem. Phys.*, **104**, 1040 (1996).
- [18] P.J. Hay, W.R. Wadt. *J. Chem. Phys.*, **82**, 270 (1985).
- [19] www.chemcraftprog.com.
- [20] S.E. Lappi, W.B. Collier, S. Franzen. *J. Phys. Chem. A*, **106**, 11446 (2002).
- [21] <http://cccbdb.nist.gov/vibscalejust.asp>.
- [22] (a) V. Di Marco, G.G. Bombi. *Mass Spectrom. Rev.*, **25**, 347 (2006); (b) M.J. Keith-Roach. *Anal. Chim. Acta*, **678**, 140 (2010).
- [23] M.C. Etter. *Acc. Chem. Res.*, **23**, 120 (1990).
- [24] A.W. Addison, T.N. Rao, J. Reedijk, J.V. Rijn, G.C. Verschoor. *J. Chem. Soc. Dalton Trans.*, 1349 (1984).
- [25] K.A. Siddiqui, G.K. Mehrotra, R.L. LaDuca. *Polyhedron*, **28**, 4077 (2009).
- [26] L.-J. Zhang, X.-C. Shen, Y. Yang, H. Liang. *Acta Crystallogr. E*, **65**, m1517 (2009).
- [27] U. Pal Chaudhuri, L.R. Whiteaker, A. Mondal, E.L. Klein, D.R. Powell, R.P. Houser. *Inorg. Chim. Acta*, **360**, 3610 (2007).
- [28] L.L. Di, Y. Wang, G.W. Lin, T. Lu. *Acta Crystallogr. E*, **66**, m610 (2010).
- [29] M. Di Vaira, C. Bazzicalupi, P. Orioli, L. Messori, B. Bruni, P. Zatta. *Inorg. Chem.*, **43**, 3795 (2004).
- [30] A. Sarkar, A.K. Ghosh, V. Bertolasi, D. Ray. *Dalton Trans.*, **41**, 1889 (2012).
- [31] I. Nakagawa, T. Shimanouchi. *Spectrochim. Acta*, **20**, 429 (1964).
- [32] V. Stefov, V.M. Petruševski, B. Šoptrajanov. *J. Mol. Struct.*, **293**, 97 (1993).
- [33] (a) J.A. Lemire, J.J. Harrison, R.J. Turner. *Nat. Rev. Microbiol.*, **11**, 371 (2013); (b) J.M. Moulis. *Biometals*, **23**, 877 (2010); (c) G.F. Nordberg. *Toxicol. Appl. Pharmacol.*, **238**, 192 (2009).
- [34] L. Remy, M. Carrière, A. Derré-Bobillot, C. Martini, M. Sanguinetti, E. Borezée-Durant. *Mol. Microbiol.*, **87**, 730 (2013).